

Supplementary information

Device geometry and corresponding sample topography: Precise device geometry and corresponding sample topography for Device A, B, C. Device D is written at the same location but rotated along the crystallographic direction. Angle ϕ denotes the orientation of the nanocross with respect to the crystallographic direction ($\phi = 65^\circ$ for the given case). The nanocross is made of $1\ \mu\text{m}$ line segments surrounded by four highly transparent tunnel barriers (red squares) of width $\sim 30\ \text{nm}$. The tunnel barriers allows the nanocross to be tuned by a proximal side gate V_{sg} . We note that sidegate V_{sg2} was floating for all device measurements and not used.

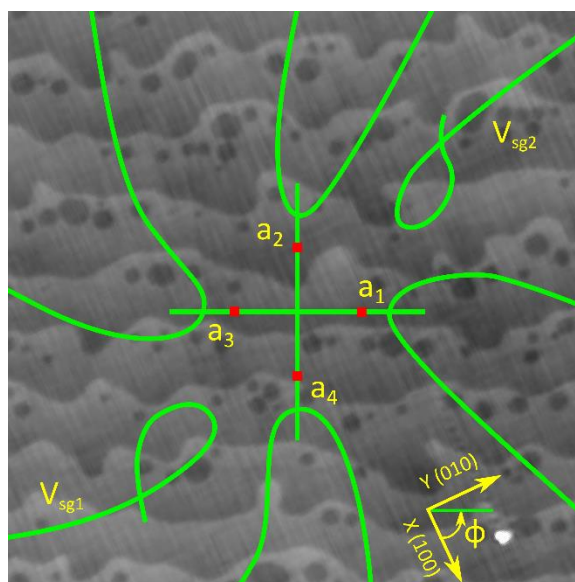


Fig. S1 The precise device geometry of the nanocross and corresponding sample topography. Four barriers of width $\sim 30\ \text{nm}$ surround the main channels of length $\sim 1000\ \text{nm}$ forming a nanocross which can be tuned by a proximal sidegate V_{sg} . Angle ϕ denotes the relative position of the nanocross with respect to the crystallographic direction.

Additional devices:

Fig. S2 and Fig. S3 shows the magnetotransport measurements for the six configurations of the nanocross of Device B and Device C respectively, written at the same spatial position and orientation on the sample as Device A. When grouped on the basis of decreasing threshold for conductance, the same configurations fall within groups I, II and III as that of Device A. Further, the transconductance spectra of group I is very similar for all three devices (Fig. 2(m-o), Fig. S2 (m-o) and Fig. S3 (m-o)). Since the configurations of groups II and III are not tuned to the insulating state, it is difficult to make a direct comparison of the corresponding transconductance spectra's. We note that the I-V curve measurements for Device B were not available. However, since the transconductance spectra of Device B is very similar to that of Device A, we can estimate the range of chemical potential for Device B. The resulting lever arm ratio¹, calculated for the conversion of sidegate voltage to chemical potential, falls within the range of lever arm ratios of devices A, C and D.

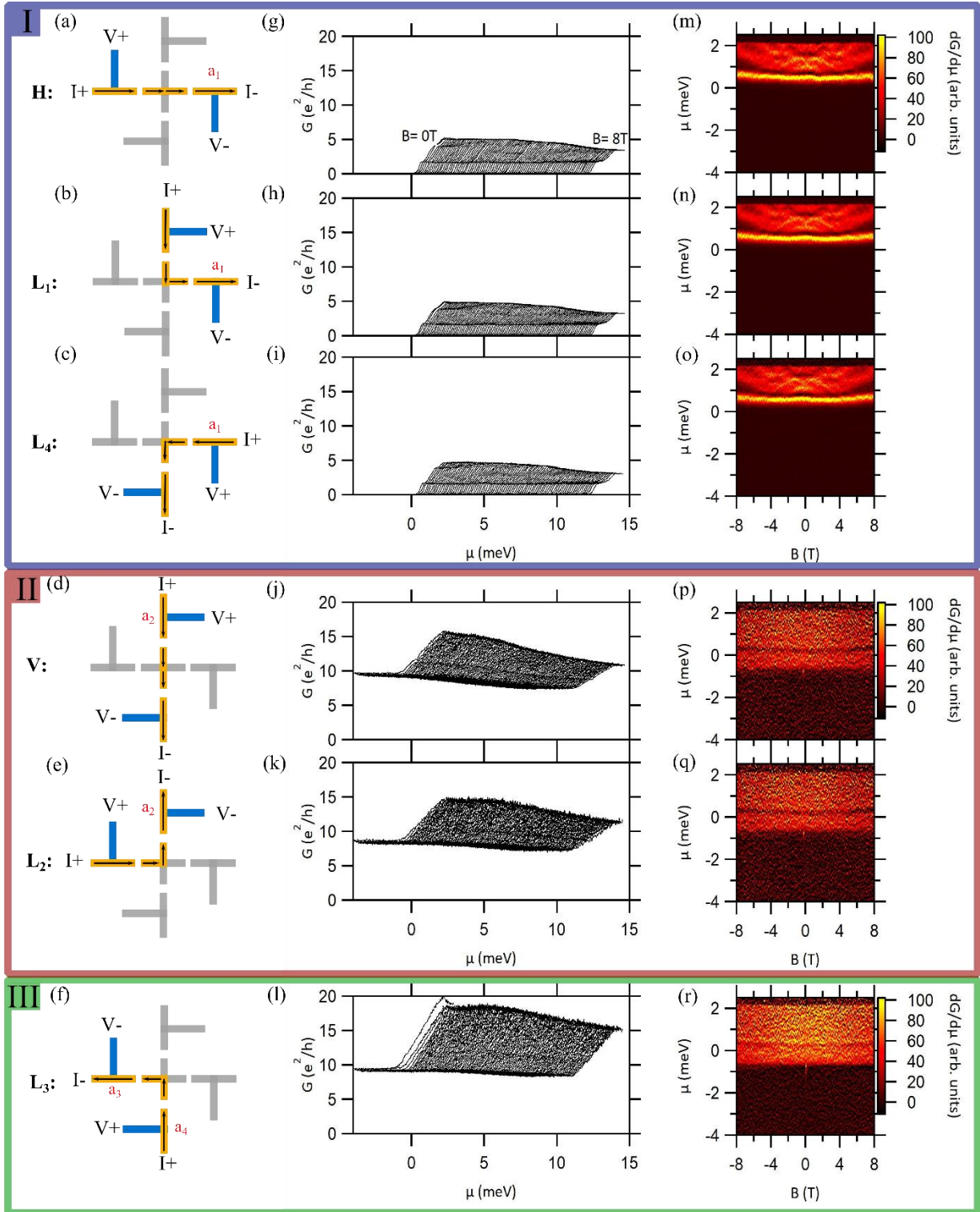


Fig. S2 Longitudinal magnetoconductance measurements for the six configurations of the nanocross of Device B, at $\phi = 65^\circ$, grouped on the basis of similar transconductance spectra. (a, d) Straight paths of the nanocross, (b, c, e, f) L-shaped paths of the nanocross, (g-l) Zero-bias longitudinal conductance, G , as a function of chemical potential μ and magnetic field B in the range 0 – 8 T for the six configurations respectively. Data is shifted along x axis for clarity, (m-r) Transconductance spectra $dG/d\mu$ shown as a function of μ and B for the six configurations.

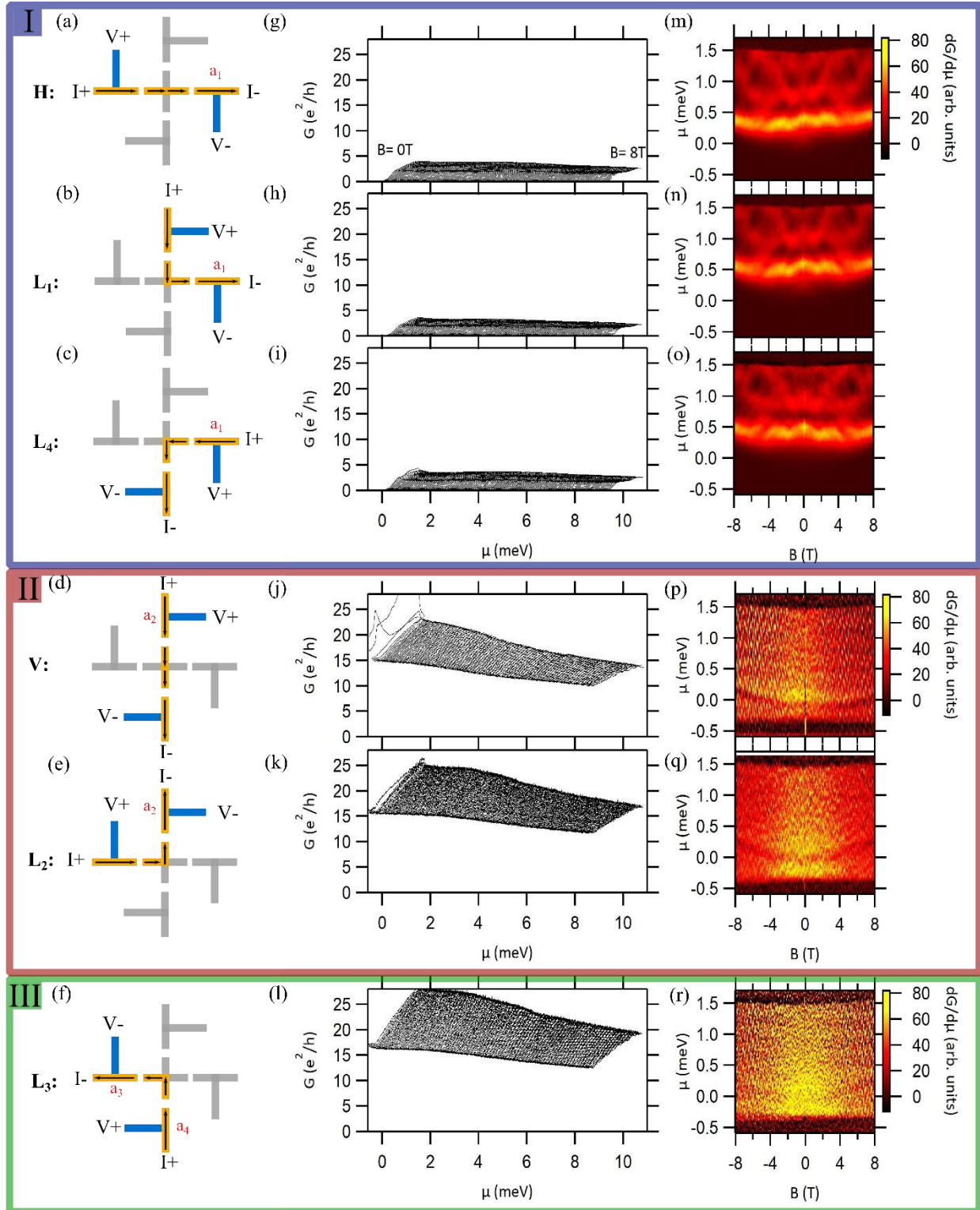


Fig. S3 Longitudinal magnetoconductance measurements for the six configurations of the nanocross of Device C, at $\phi = 65^\circ$, grouped on the basis of similar transconductance spectra. (a, d) Straight paths of the nanocross, (b, c, e, f) L-shaped paths of the nanocross, (g-l) Zero-bias longitudinal conductance, G , as a function of chemical potential μ and magnetic field B in the range 0 – 8 T for the six configurations respectively. Data is shifted along x axis for clarity, (m-r) Transconductance spectra $dG/d\mu$ shown as a function of μ and B for the six configurations.

Calculation details for Fig. 4(c):

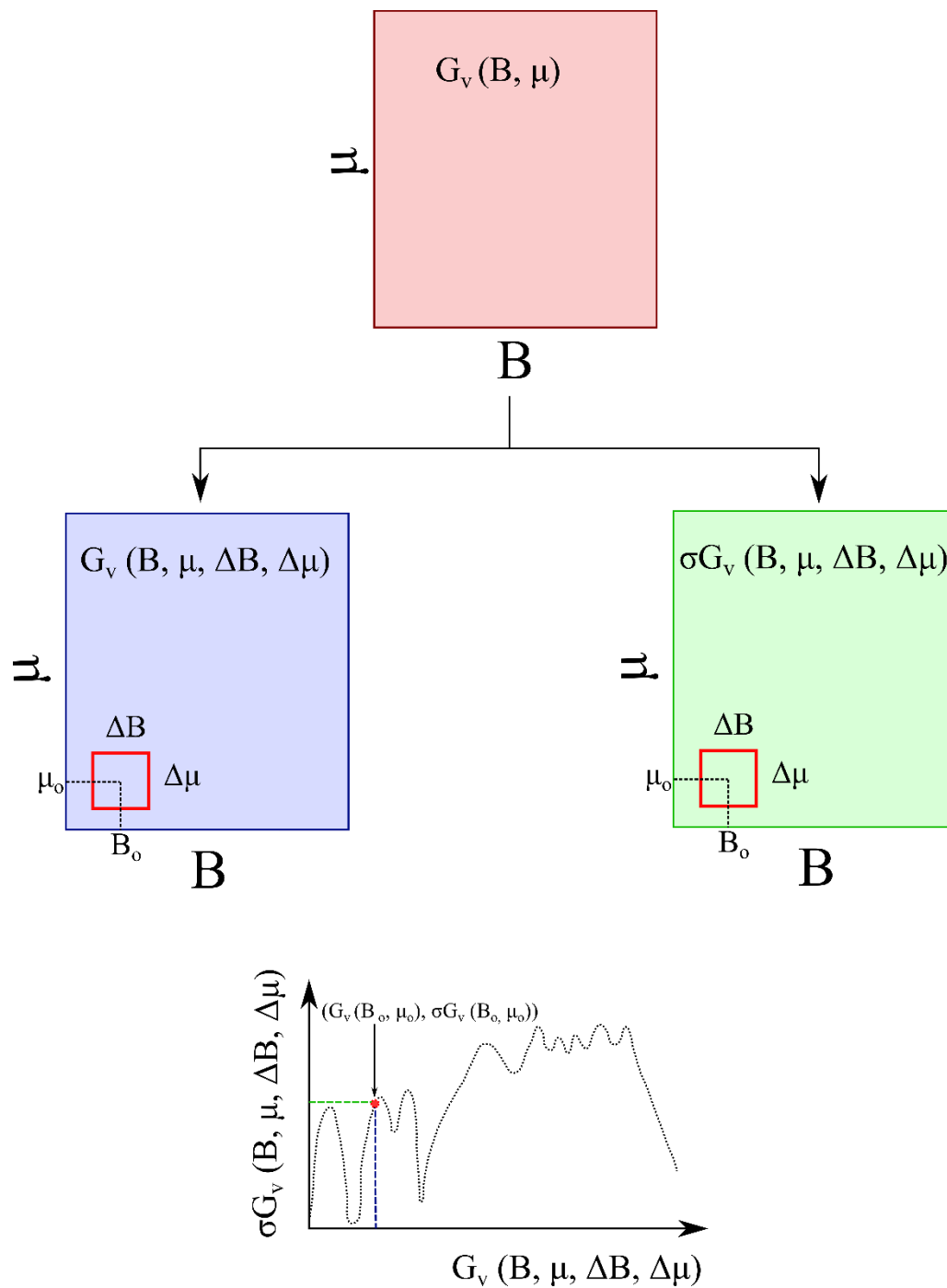


Fig. S4 Pictorial explanation of the extraction procedure for the standard deviation of G_v versus mean value of G_v plot (Fig. 4(c)). The standard deviation, σG_v , and mean value of G_v , is extracted from the G_v intensity map (Fig. 4(a)) as a function of magnetic field, B , chemical potential, μ , and arbitrary widths ΔB and $\Delta \mu$ along the x axis and y axis respectively. The standard deviation (σG_v) is finally plotted as a function of the mean value of G_v . Boxes are not scaled and points red dot does not refer to the actual data position.

Tiling rules for tetragonal domains in SrTiO₃:

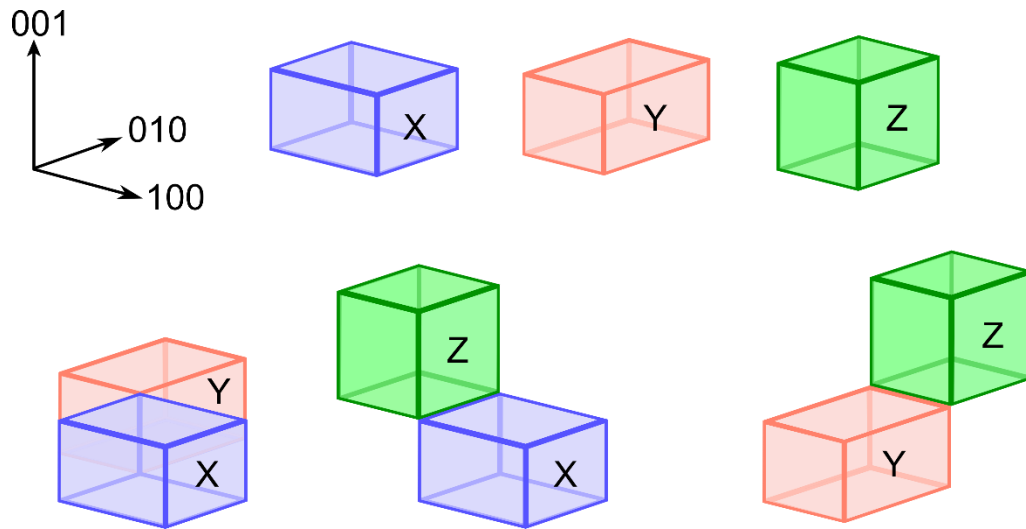


Fig. S5. Tiling rules for tetragonal domains in SrTiO₃. The X, Y and Z domains are along the (100), (010) and (001) directions respectively. According to the tiling rules, the boundary between X and Y domains should lie at 45° or 135°, between Z and X domains 0° and between Z and Y domains at 90°. The degree of tetragonality is typically $\frac{c}{a} \sim 1 + O(10^{-3})$.

References

1. A. Annadi, G. Cheng, H. Lee, J.-W. Lee, S. Lu, A. Tylan-Tyler, M. Briggeman, M. Tomczyk, M. Huang, D. Pekker, C.-B. Eom, P. Irvin and J. Levy, *Nano Lett*, 2018, **18**, 4473-4481.